Lateral Optical Sensor with Slip Detection of Natural Objects on Moving Conveyor

Kok-Meng Lee, Fellow, *IEEE* and Shaohui Foong, Member, *IEEE*

Abstract—**This paper presents a method to determine the 2D profile and velocity of an object on a moving conveyor from a lateral optical sensor that consists of an orthogonal pair of line array (LA) scanners. Unlike most LA scanners which are designed to provide a 2D image of a static object, the lateral optical sensor presented here offers an additional and practical means to detect object slippage on the conveyor in real time. We illustrate numerically the effectiveness of this sensing method with two illustrative examples. The first simulates the 2D boundary of a geometrically well-defined object on an accelerating conveyor, which offers intuitive insights on the effects of conveyor dynamics and object slippage on the accuracy of the 2D boundary measurement. The second demonstrates the application of the lateral optical sensor as a real time feedback sensor for active singulation of natural objects.**

I. INTRODUCTION

Line scanners have widely been used in document reproduction and dimensional measurement. Although they are well known for their ability to offer high-resolution images with inexpensive sensors in limited viewing distance, their applications for industrial automation are under exploited. In applications such as part-presentation on moving conveyors, lateral position and velocity are essential real-time information for subsequent robotic or automated mechanical handling. Motivated by practical problems commonly encountered in food processing where natural objects must be handled repetitively at high-speed, this paper introduces a new method (referred to here as a lateral optical sensor) to detect and compensate for object slippage on the conveyor while reconstructing the object boundary in real time without utilizing an optical camera. To facilitate the illustration, the sensing method is presented in the context of mechanical singulation.

Mechanical singulation [1] [2] involves the separation of randomly spaced objects such that a minimum specified distance between neighboring objects is maintained after singulation. Conventional singulating systems are commonly passive. They remain in constant-speed motion as the arrival conveyor moves object after object between the two sets of continuously rotating fingers. Hence even if there is no object in the unsingulated region, the system will be

oblivious and remain in motion. Active singulation, which requires only a small number of finger-sets, not only eliminates excess movement when the object is not completely in the specified region or there are no objects to be singulated, but also objects can be more accurately singulated and equally spaced on the next conveyor as contact forces on the object can be more consistently predicted. More importantly, in handling of live objects, active singulation effectively minimizes visual stimuli of the rotating fingers and thus could drastically reduce injuries due to unpredictable escape behaviors. The success of active singulation, however, relies on the ability to detect the arrival between objects and estimate the spacing between incoming objects in poor lighting conditions in order to manipulate the speed of the singulator and conveyors.

The simplest scheme to activate the singulating fingers when an object enters the specified region is to use a point proximity sensor. Unlike engineering objects which often have well-defined boundary with straight edges or geometrically simple curves, natural objects (such as food products and live objects for meat processing) do not have a well-defined shape. As a result, the activation of the point sensor is generally inconsistent due to the irregularity of the body shape, and the possibility of object slippage or voluntary motion (in the case of live products). Any accidental activation of the point sensor will cause the singulation system to activate earlier than expected. For this reason, we develop a method based on a combination of optical line-array sensors for active singulation of randomly spaced objects.

Line sensors have been used as a lateral position detection device to detect lane markers on roads [3] for applicative use in autonomous navigation. The rapid scanning of the line sensor estimates both the heading and position of the car within the lane markers. In biometrics, small scale line sensors are implemented within a fingerprint verification system [4]. In addition, an array of PIN photodiodes can be used as a depth measurement tool to obtain a 3D topological image [5]. With the exception of [6] where a single-line CCD camera has been successfully used to measure the spin rate of a specially-marked golf ball moving at high speed, most of the line array scanners are mobile in applications, and designed to provide a 2D image of a static object.

The remainder of this paper is organized as follows:
1) We present a lateral optical sensor to construct the 2D boundary of a natural object on a moving conveyor from discrete profile scans. This sensor, which uses a pair of

978-1-4244-1647-9/08/$25.00 ©2008 IEEE.   **329**

line array scanners mounted perpendicularly, exploits the fast scan rate of the photoelectric sensors to detect discrepancies between the position/velocity of the object and the conveyor.

2) We illustrate the use of this sensing method (which offers a practical means to detect and compensate for object slippage on conveyor) to perform object-based location calibration.

3) To demonstrate the effectiveness of this method, we offer two illustrative examples. The first example investigates numerically the effects of conveyor dynamics and object slippage due to conveyor acceleration through comparisons of the reconstructed the side profiles of a well defined geometrical object. The second example examines the feasibility of implementing this method in a process of active singulation in an automated natural object handling application. Key issues include maintaining object throughput and precise triggering

II. OPTICAL LINE ARRAY (LA) SENSORS

An optical emitter-receiver pair (or a point sensor) is similar to an on-off switch. When the light beam from the emitter is collected unobstructed by the receiver, it 'completes' a circuit and is said to be "on". Conversely when the beam is obstructed and does not reach the intended receiver, the sensor is "off". This property coupled with the fast scan rate allows the optical sensor for use as a non-invasive triggering mechanism to detect the proximity of (geometrically well-defined) engineering-objects with high degree of accuracy and reliability. However, natural objects do not have a well-defined shape; activation using a point sensor is generally inconsistent due to the irregularity of the body shape. Any accidental activation of the point sensor will send a triggering signal earlier than expected.

A. Sensor Formulation

An effective alternative to overcome the shortcomings of a point sensor is the use of a line array (LA) sensor shown in Figs. 1(a) and 1(b). The LA sensor may be installed in horizontal and vertical configurations. For simplicity, we denote the horizontally and vertically placed LA sensors as LAH and LAV respectively, and k for $t=kT$.

The LA sensor consists of N photoelectric sensors (or emitter-receiver pairs) spaced equally apart along a straight line. The emitters are pulse modulated at preset frequencies so that light beams do not activate the adjacent receivers and also prevent ambient light from corrupting the beam signals. This modulation also allows the sensor to function in a variety of lighting conditions. The status of the ith pixel p_i on the LA sensor at $t=kT$ (where T is the sampling time) can be written as

$$s(p_i, k) = \begin{cases} 0 & \text{if beam was made} \\ g & \text{if beam was blocked} \end{cases} \quad 1 \le i \le N \quad (1)$$

Without loss of generality, we assume that the sensor is binary ($g=1$). The principle discussed in this paper can be applied to grey-level sensor once an appropriate threshold is determined and normalized.
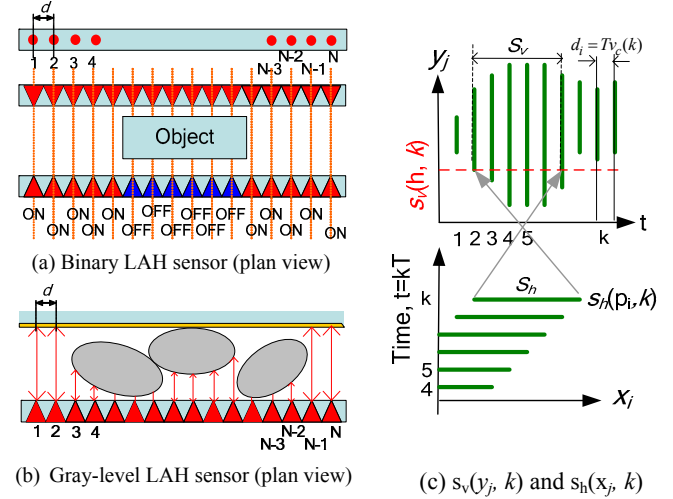

(a) Binary LAH sensor (plan view)

(b) Gray-level LAH sensor (plan view)

(c) $s_v(y_j, k)$ and $s_h(x_j, k)$

Fig. 1 Optical Line Sensor

In the following discussion, we assume that the conveyor moves in one direction, $v_c(k) \ge 0$. For an object entering a LA sensor, the leading edge E_L can be located by testing the neighbors of the ith pixels:

$$\text{If } s(p_m, k) = \begin{cases} 0 & i < m < i + \beta \\ 1 & i - \beta < m \le i \end{cases} \quad \text{then } E_L(k) = i \quad (2a)$$

where m is a neighbor point; and β is an integer threshold to be defined. This 0-to-1 transition provides a means to locate the 1st beam blocked by the object when it enters the detectable region of a LAH. Similarly, the location of the trailing edge E_T is found by using a neighbor point n as follows:

$$\text{If } s(p_n, k) = \begin{cases} 1 & i < n < i + \beta \\ 0 & i - \beta < n \le i \end{cases} \quad \text{then } E_T(k) = i \quad (2b)$$

The trailing edge is a 1-to-0 transition that signals the last beam blocked by a (completely filled) object. An odd number of edge transitions indicate an object enters or leaves the LAH detectable region; a sequence that begins with a leading edge signals an object is entering while that ends with a trailing edge signals the object is leaving.

The span S (or the number of pixels between a leading edge and a trailing edge) can be written as

$$S(k) = E_{L/T}(k) - E_{T/L}(k) + 1 \quad (2c)$$

where the subscripts "L/T" and "T/L" denote the E_L-to-E_T transition and the E_T-to-E_L transition respectively. The span is the continuous beams blocked between E_L and E_T inclusive. A vertical span S_v sequence, which can be obtained from the LAV, gives the object boundary and/or the space above and below the object). The horizontal span S_h (obtainable directly from the LAH) can be used to determine an object's cross sectional length and/or spacing between two adjacent objects.

LA in Vertical Configuration

When the LA sensor is placed vertical and perpendicular to the motion of the object, a side profile of the object can be scanned as the object passes it. The upper time-plot in Fig.

330

1(c) shows an example data set captured by the LAV, where the data is a mirror image of the actual object. For a small sampling time T,

$$v(t) \approx v(k) \qquad \text{when } kT \le t < (k+1)T \qquad (3)$$

A 2D image $\mathbf{P}(x, y)$ can be constructed from the LAV data with elements given by (4a, b)

$$x_i \approx \hat{x}_i = v_c(k)T \text{ and } P(x_i, y_j) = s_v(y_j, k) \qquad \text{(4a, b)}$$

where $v_c(k)$ is the conveyor velocity. The image fidelity obtained with (4a, b), however, relies on the two assumptions: 1) The conveyor speed $v_c(k)$ is known and T is small; and 2) the object does not move or slip relative to the conveyor.

LA in Horizontal Configuration

Unlike LAV data where the spacing between two adjacent columns is velocity dependent, the repetitive LAH snapshots offer a means to measure the absolute velocity of the object by tracking the motion of the leading or trailing edge between two consecutive snap-shots. The lower time-plot in Fig. 1(c) shows an example sequence of data sets captured by a LAH. As a 2nd order approximation, the object velocity $\tilde{v}(k)$ can be estimated from the time derivative of the leading (or trialing) edge motion between consecutive instants:

$$\tilde{v}(k) = \left[3E_{L/T}(k) - 4E_{L/T}(k-1) + E_{L/T}(k-2) \right] d_x / 2T \qquad (5)$$

where d_x is the spacing between adjacent pixels of the LAH. Moreover, the ability to observe discrepancies between the object velocity and the conveyor velocity allows the detection of slipping between the object and conveyor. Slipping is said to occur if

$$v_c\left[(k-1)T \le t < kT \right] > 0 \text{ , and}$$

$$E_{L/T}(k) < E_{L/T}(k-1) + \text{int}\left| v_c T / d_x \right|. \qquad \text{(6a,b)}$$

where int($\bullet$) denotes the integer of $\bullet$.

LAV/LAH Pair for Object-based 2D Image Calibration

For applications such as active singulation, the object may slip relative to the conveyor surface and thus, the spacing between two adjacent columns of the LAV data can no longer be found as a function of the conveyor $v_c(t)$ alone. However, if an additional LAH is installed orthogonal to the LAV, the repetitive snap-shots of a horizontal line segment offer the sensor pair would offer a practical means to perform an ***object-based location calibration***. It is then possible to make alterations to (4a, b) such that the image constructed from the LAV is undistorted as a result of slipping.

We make the following assumptions in the object-based location calibration:

1) The conveyor speed is measurable and known; this assumption allows slipping to be detected from (6).

2) The LAH must detect the leading and trailing edges of the object before the LAV begins and ends its line-scan respectively. The rationale for this can be illustrated with the aid of Fig. 2. As shown in Fig. 2, if the object is first scanned vertically by LAV before the LAH detects the first leading edge $E_L(k)$ there will be no basis to estimate

the spacing between LAV columns scanned before $t=kT$. On the other hand, if the LAH leading edge can be tracked as illustrated in Fig. 2(c) before the LAV makes its first scan of the object, the information of the LAH edge transitions $E_L(t \ge kT)$ can then be used to estimate every spacing between columns scanned by the LAV.
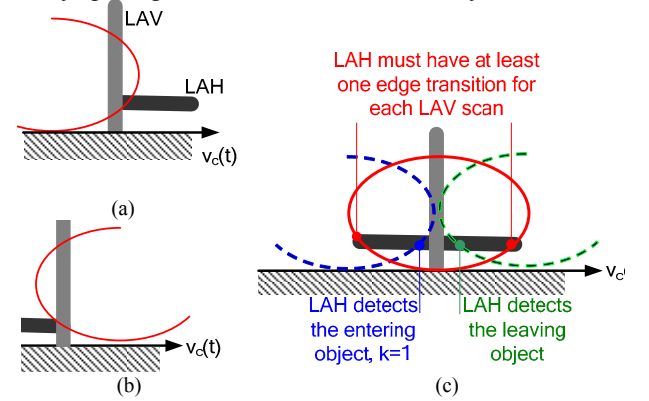

Fig. 2 (Side view)

3) The LAH and LAV are fixed relative to each other and that there is at least an LAH edge transition (leading or trailing) when the LAV makes a scan. This is to guarantee every space between columns scanned by the LAV can be estimated.

As graphically illustrated in Fig. 1(c), both sensors construct a binary image that increases in size with increasing time. While the images captured by both sensors are different dimensionally, they can be related to each another by virtue of their geometric configuration, the known sampling interval T, and the knowledge of the conveyor velocity $v_c(t)$. The followings are relationships derived with the aid of Fig. 1(c), where the upper and lower time plots correspond to the LAV and LAH data respectively:

1) The pixel values registered in the LAH are repetitions of the $\text{int}(h/d_y)^{\text{th}}$ pixel of the LAV:

$$s_h(p_i, k) = s_v\left[\text{int}(h/d_y), \text{Int}(T_d/T) + (k-i) \right] \qquad (7)$$

where $T_d = d_s / v(0)$.

2) The span S_h (or the number of pixels between the leading and trailing of the object inclusive) obtained from LAH is given by

$$S_h(k) = \left[E_L(k) - E_T(k) + 1 \right]\Big|_{LAH} \qquad \text{(7a)}$$

Unlike the LAH which provides an instantaneous snap-shot, the same horizontal span can be obtained from the LAV data but is velocity dependent as it must be deduced from data made up of more than one vertical scans:

$$\hat{S}_h(k) = \text{int}\left\{ \frac{1}{Td_x}\left[x_n(k-\ell) - x_m(k) \right]\Big|_{y_i = h} \right\}_{LAV} \qquad \text{(7b)}$$

where l is the number of sampling periods between the leading and trailing edges on the LAV.

B. Data Representation

Unlike conventional line proximity sensors which only detect if any of the light beams are blocked as the sole

binary (digital) output, we introduce here a hybrid scheme to utilize a combination of digital and analog output signals as a function of the beams individual instantaneous states to convey a variety of measurements and information. Such signals are preferred as they can be directly integrated in existing control schemes in motion controllers as a triggering device (digital output) or independent measurement sensor (analog output) as compared to transmitting individual beam states that require further processing by a computer.

The individual binary states of the LA sensors can be represented in the hexadecimal (Hex) system using one character (0…F) to register the states of the 4 pixels. Tables 1 and 2 show an example displaying the beam states of a 8-pixel LAV/LAH pair along with their HEX representation and measurement features. Table 1 tabulates the LAV data, where each column line-scans the passing object vertically. On the other hand, the beam states of the LAH (collinear with the 3rd beam of the LAV) are given in Table 2 showing the horizontal snap-shots.

Table 1: Example LAV data $s_h(p_i,k)$

k=	1	2	3	4	5	6	7	8
p_8	0	0	0	1	1	0	0	0
p_7	0	0	1	1	1	1	0	1
p_6	0	1	1	1	1	1	1	1
p_5	1	1	1	1	1	1	1	1
p_4	1	1	1	1	1	1	1	0
p_3	0	1	1	1	1	1	0	0
p_2	0	0	1	1	1	1	0	0
p_1	0	0	0	1	1	0	0	0
Hex	18	3C	7E	FF	FF	7E	38	70
E_L	5	6	7	–	–	7	6	7
E_T	4	3	2	–	–	2	4	5
S_v	2	4	6	–	–	6	3	3
N_T	2	2	2	0	0	2	2	2

Table 2: Example LAH $s_h(p_i,k)$, g=1 (binary)

k	p_1	p_2	p_3	p_4	p_5	p_6	p_7	p_8	Hex	E_L	E_T	S_h
13	0	0	0	0	0	0	0	0	00	0	0	0
12	0	0	0	0	0	0	0	1	01	–	8	–
11	0	0	0	0	0	0	1	1	03	–	7	–
10	0	0	0	0	0	1	1	1	07	–	6	–
9	0	0	0	0	1	1	1	1	0F	–	5	–
8	0	0	1	1	1	1	1	0	3E	7	3	5
7	0	1	1	1	1	1	0	0	7C	6	2	5
6	1	1	1	1	1	0	0	0	F1	5	–	–
5	1	1	1	1	0	0	0	0	F0	4	–	–
4	1	1	1	0	0	0	0	0	E0	3	–	–
3	1	1	0	0	0	0	0	0	C0	2	–	–
2	1	0	0	0	0	0	0	0	A0	1	–	–
1	0	0	0	0	0	0	0	0	00	–	–	–

C. Slip Detection – Illustrative Example 1

Slipping would result in velocity discrepancies between the object and the conveyor. If there is insufficient friction between the object and conveyor surface, slipping will occur when the conveyor acceleration exceeds the critical value:

$$a_c = \mu g \qquad (8)$$

where μ is the coefficient of friction between the object and the conveyor surface. We illustrate an example (Fig. 3) to offer some insight to the effects of slip in addition to the following factors on the accuracy of the optical LA sensor pair; 1) the variation of conveyor speed, and 2) the unknown object velocity relative to the conveyor.

Figure 3 shows the (right-angled triangular) test-object on the conveyor (which travels initially at a constant velocity, and then uniformly accelerates to a specified higher velocity) as the object passes through the sensor pair. The conveyor dynamics is assumed to be 1st order of the form:

$$\tau dv_c / dt + v_c(t) = u(t) \qquad (9)$$

where τ is the time constant; and $u(t)$ is the normalized controlling input to the conveyor.

Parameters
$N= M=n=64$
$d_x=d_y=d_s$
$=5mm$
$h=40\ mm$
$T =10ms$
$\tau =0.1$s
$\mu=0.3$

Cycle time prediction
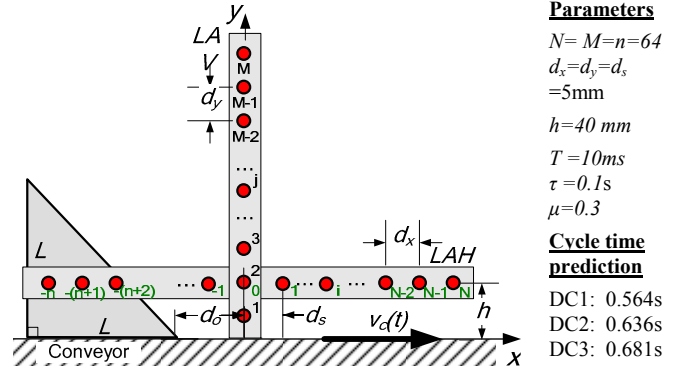DC1: 0.564s
DC2: 0.636s
DC3: 0.681s

Fig 3 Schematics illustrating Example 1

A MATLAB program was written to simulate the data representation of the LAH/LAV sensor pair. We study the effects by comparing the results against two common design configurations (DC's); a point sensor, and a single LAV sensor. The three DC's are configured as follows:

DC-A: The conveyor velocity is assumed to be constant and not measured; $v(t) = \bar{v}_c$.

DC-B: A non-slip condition is assumed; $v(t) = v_c(t)$. The conveyor speed is measured with an encoder and a point sensor, which locates the 1st leading edge, E_T but does not have the ability to track its motion.

DC-C: The object and conveyor velocities, $v(t)$ and $v_c(t)$, are independently measured to detect the condition of slip. The LAH/LAV sensor pair is used to estimate the velocity of the object and reconstruct its image.

In all three DC's, a LAV sensor is used to construct the image of the object. Other parameters used in the simulation are given in Fig. 3; the values characterizing the sensors are modeled after the off-the-shelf line sensors manufactured by Banner Engineering [7]. The results are summarized in Fig. 4. Figures 4(a) and (b) compare the velocity and the displacement of the object among the three DC's. By locating the trailing edge of the LAV at each sampling instant, the boundary of a mirrored 2D image **P**(x,y) of the test object can be obtained. Figure 4(c) compares the image boundary computed using (4a,b) against those taking into account the conveyor dynamics (9) and the conditions of slipping (6) and (8). The resulting timing errors in the *x* direction as defined below are summarized in Fig. 4(d):

$$error(k) = |x(k) - \hat{x}(k)| \quad \text{where } \hat{x}(k) = T\sum_{i=0}^{k-1} \tilde{v}(i)$$

Some observation can be made from the comparison:

- Provided that the object does not slip, the object displacement can be deduced from (4a, b). However, the

DC-A does not take into account the conveyor dynamics during acceleration; the *x*-positional error grows as the object accelerates with the conveyor. This results in a geometrically distorted 2D image in the *DC-A*.

- The *DC-B* uses the conveyor velocity to estimate the spacing between the LAV column scans. The failure to detect slipping between the object relative to the conveyor surface leads to a constant steady state error in the 2D image constructed in the *DC-B*.

- In *DC-C*, the absolute velocity of the object can be estimated using (5). In addition, the location and duration of slipping can be obtained by comparing the LAH estimated velocity of the object and the measured conveyor velocity using (6). The LAH estimated velocity (5) can be applied to correct profiles (4a, b) that have been distorted by slipping or relative motion of the object as well.

(a) velocity   (c) 2D object boundary

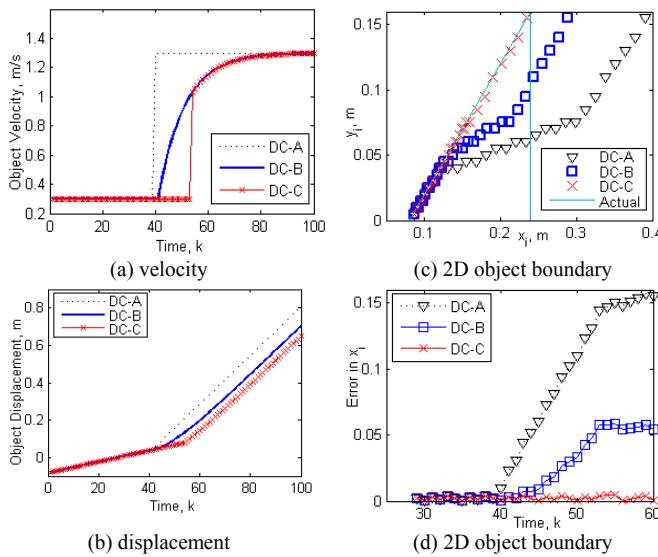(b) displacement   (d) 2D object boundary

Fig. 4 Simulated results of Example 1

In summary, the LAH offers a practical means to estimate the absolute velocity, detect slipping, and correct the 2D image boundary of the object. From the 2D image, other pertinent geometrical features of the object such as the centroid can be obtained using existing imaging techniques. These attractive features offered by a LAH/LAV sensor pair can neither be obtained from a point sensor nor a single LAV sensor.

III. ACTIVE SINGULATION APPLICATION – EXAMPLE 2

In high-speed food processing, natural objects (such as agricultural, poultry or meat products) must be singulated into equal spaces for repetitive operations executed mechanically. Since it is impractical to label or tag individual natural objects, non-contact optical LA sensors are a logical choice. Unlike a conventional singulator as shown in Fig. 5(a) [1] [2] where a high density of fingers is rotated continuously, active singulation requires only a small number of finger-sets as illustrated in Fig. 5(b), which uses the LAH/LAV sensor feedback to synchronize the drum motion with the arrival of each object. Active singulation

eliminate excess movement when the object is not completely in the specified region, and thus, active singulation has significant potentials in live-product handling applications.

Figure 5(c) shows an example singulation system, where objects of varying spacing are fed into a singulator from the 1st conveyor (C1) and exit on the 2nd conveyor (C2). The sensor pair uses the LAH to determine the spacing d_s between the object B_1 being singulated and the next incoming object B_2, and the LAV to detect the front edge of B_2. The singulating fingers execute when the front edge of B_1 reaches a critical distance D_c (from the centerline of the drums as shown in Fig. 5c) allowing space to avoid collision with the barrier fingers on the drums. This position corresponds to E_D on the LAH. As B_1 is being singulated, the rotational motion of the drums will accelerate B_1 towards C2 creating a spacing between B_1 and B_2 immediately after which the LAV scans the B_2 as it passes through. The LAH/LAV data is then fed back to manipulate the velocity for controlling the conveyors and the singulating fingers; v_1, v_2 and ω.

(a) Passive singulator

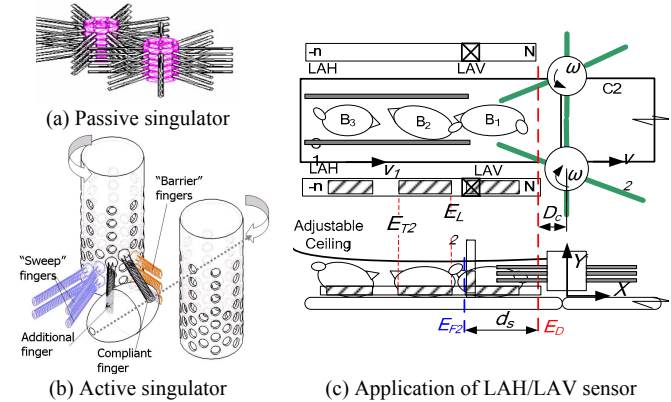(b) Active singulator   (c) Application of LAH/LAV sensor

Fig. 5 Singulation process

For simplicity, we focus on the control scheme built around the conveyor C1, which has the dynamics given in (9), to illustrate the application of the LAH/LAV sensor pair for active singulation of the objects. The objective of the repetitive control scheme (Fig. 6) is to present an object sequentially to the singulator precisely at a specified cycle time of t_c second, where the desired velocity trajectory v_d is computed in real time as follows:

$$v_d(t) = d_x \left(E_D - E_T\right) / \left(t_c - t\right) \qquad \text{for } 0 \le t < t_c \qquad (10)$$

As shown in Fig, 6, this desired object velocity is fed into the velocity controller of C1, the acceleration of which is continuously monitored to access if slippage occurs between the object and conveyor surface using (6). When the object passes through the LAV, it triggers the rotation of the fingers onto C2. An example consisting of five unequally spaced objects (Fig. 7) has been simulated to illustrate the active singulation process described above. Practical operating limits of the C1 velocity put a bound on the object spacing (front edge to front edge) if the desired cycle time t_c is to be maintained. The maximum object spacing corresponds to the case when the conveyor is commanded to accelerate from the lowest velocity v_{min} (at the start of the

cycle) immediately to highest velocity v_{max}. Similarly, the minimum object spacing is bound by the opposite case when $v_C = v_{max}$ at the start of the cycle and is commanded to v_{min} immediately. Taking into account the conveyor dynamics and object slippage, the conservative upper and lower bounds of the object spacing are:

$$d_{\min} \leq d_s \leq d_{\max} \qquad (11)$$

where

$$\frac{d_{\max}}{(v_{\max}-v_{\min})\tau} = \frac{(t_c/\tau)v_{\min}}{v_{\max}-v_{\min}} + \left[\frac{t_c-t_s}{\tau} + e^{-t_c/\tau} - e^{-t_s/\tau}\right] \qquad 11(a)$$

$$\frac{d_{\min}}{(v_{\max}-v_{\min})\tau} = \frac{(t_c/\tau)v_{\max}}{v_{\max}-v_{\min}} - \left[\frac{t_c-t_s}{\tau} + e^{-t_c/\tau} - e^{-t_s/\tau}\right] \qquad 11(b)$$

and

$$\frac{t_s}{\tau} = \begin{cases} 0 & \text{if } \mu g \tau \geq v_{\max} - v_{\min} \\ -\ln\left(\dfrac{\mu g \tau}{v_{\max} - v_{\min}}\right) & \text{otherwise} \end{cases} \qquad (11c)$$

Using the values given below,

$$\mu=0.5;\ \tau=0.25\text{s};\ v_{max}=2\text{m/s};\ \text{and}\ v_{min}=0.05\text{m/s}$$

the upper and lower bounds of the object spacing as a function of desired cycle time are graphed in Fig. 7. It is noted that a cycle time of less than 0.5 second is not sustainable because of the 1st order lag of the conveyor system. In addition, the conveyor C2 provides an additional degree of freedom to help meet the cycle time requirement if the object spacing on C1 exceeds the bound.
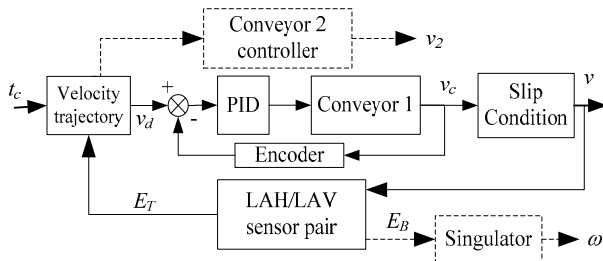

Fig. 6 LAH/LAV-based control scheme

d_{Si} (where i=1, 2, 3, 4, 5) are given by
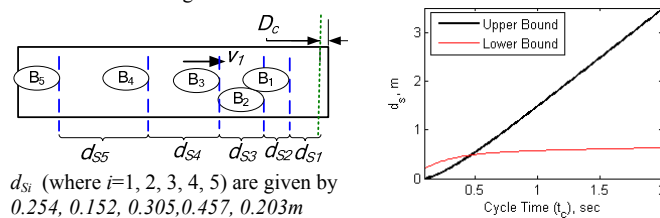*0.254, 0.152, 0.305,0.457, 0.203m*

Fig. 7 Parameters used in Simulation

The location of the object at each time step is shown in Fig 8(a) depicting the motion of each object during each of the five singulation cycles. The corresponding velocity and acceleration of the conveyor are shown in Figs 8(b) and 8(c) respectively. In this simulation, the maximum velocity of the conveyor is capped at 2 m/s, and the minimum velocity is set at 0.05m/s in order to avoid static friction of C1. As seen in Fig. 8(d), the object displacement does not decrease linearly as a result of the first order conveyor dynamics and slippage that occurs as a result of varying conveyor speeds. It is noted that the conveyor velocity increases as the object approaches E_D due to the decreasing magnitude of $(t_c - t)$ in (10).

IV. CONCLUSION

We have presented a new sensing method based on the principle of a line array scanner to construct a 2D profile of an object on a moving conveyor. The method utilizes a pair of line array sensors to capture the lateral profile as well as the velocity of the object. As illustrated with a practical example, the lateral optical sensor exploits the fast scan rate of the photoelectric sensors to detect discrepancies between object position/velocity and conveyor position/velocity, which makes it a useful tool for applications where slip detection and compensation are required in real-time. Lastly, we have also applied the lateral optical sensor for real-time velocity feedback and as a precise triggering device in an active singulation process.
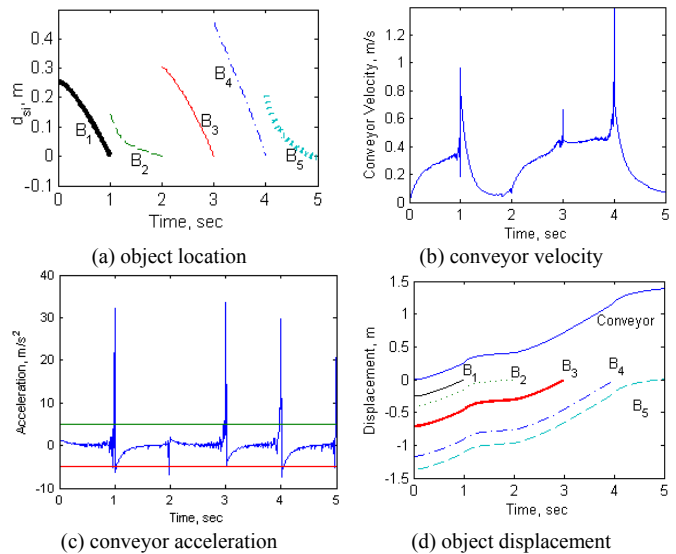

(a) object location   (b) conveyor velocity

(c) conveyor acceleration   (d) object displacement

Fig. 8 Simulated results of Active singulation (t_c=1s)

REFERENCES

[1] K.-M. Lee, R. Gogate, R. Carey, "Automated Singulating System for Transfer of Live Broilers," IEEE ICRA, May 1998.

[2] K.-M. Lee, "Design Criteria for Developing an Automated Live-Bird Transfer System," IEEE ICRA, Apr 2000

[3] Y. Narita, S. Katahara and M. Aoki, "Lateral Position Detection using Side Looking Line Sensor Cameras," Proceedings of IEEE Intelligent Vehicles Symposium, pp 271-275, Jun 2003.

[4] N. Galy, B. Charlot and B. Courtois, "A Full Fingerprint Verification System for a Single-Line Sweep Sensor," IEEE Sensors Journal, vol 7, no. 7, Jul 2007.

[5] A. Nemecek, K Oberhauser, G. Zach and H. Zimmermann, "Distance Measurement Line Sensor with PIN Photodiodes," IEEE Sensors EXCO, Oct 2006.

[6] T. Kadowaki, K. Kobayashi and K. Watanabe, "Rotation Angle Measurement of High-speed Flying Object," SICE-ICASE Conference, Oct 2006.

[7] Banner Engineering, "A-GAGE® EZ-ARRAY™ Series", http://www.bannerengineering.com.

334